J Mater Sci (2015) 50:7998–8006
DOI 10.1007/s10853-015-9365-6

Effective method for the synthesis of pimelic acid/TiO_2 nanoparticles with a high capacity to nucleate β-crystals in isotactic polypropylene nanocomposites

J. A. Gonzalez-Calderon[1] · Javier Vallejo-Montesinos[2] · J. M. Mata-Padilla[3] · Elías Pérez[4] · A. Almendarez-Camarillo[1]

Received: 24 May 2015 / Accepted: 18 August 2015 / Published online: 27 August 2015

Abstract Functionalized titanium dioxide (TiO_2) nanospheres with pimelic acid (TiO_2–PA) were synthesized through a novel and effective route, where the goal was to promote a high percentage of β-crystal into a matrix of isotactic polypropylene (iPP) by the use of low amount of nucleating agent. The successful chemical attachment of pimelic acid onto the TiO_2 surface was indicated by the presence of a new band at 1575 cm^{-1} and an increase in the thermal stability of the PA of approximately 200 °C, which were observed through infrared spectra and thermogravimetric techniques, respectively. The iPP nanocomposite was analyzed by differential scanning calorimetry and wide-angle X-ray diffraction in order to identify β-crystals. An exothermic peak at 152 °C and a diffraction peak at $2\theta = 16.2°$ confirmed the ability of the TiO_2–PA nanoparticles to promote the β-crystal phase in the iPP nanocomposite even at low percentages (0.1 % w/w).About 85 % of β-crystal content was promoted with the TiO_2–PA particles, that was significantly higher than the 25 % obtained by unmodified TiO_2 particles. Moreover, from visco-elastic analysis, it is evident that TiO_2–PA particles help to improve the dissipation energy by effect of the promoted β-crystal phase in the polymer composites. Likewise, the AFM images provide evidence of the incompatibility of TiO_2 particles with the iPP matrix showing protruding reliefs in comparison with the homogeneous topography of the iPP/TiO_2–PA composite. This results were confirmed by SEM, where the exclusion of TiO_2 particles was evident.

Introduction

Isotactic polypropylene (iPP) is the most common commercial form of polypropylene because of its mechanical resistance due to its crystallinity. iPP can crystallize into different crystalline phases depending on its stereochemical structure, molecular weight, temperature of crystallization, pressure applied during the crystallization process, and also by adding additives [1–10]. The main crystalline phases are known as α-, β-, γ-, and mesomorphic or smectic form [2–10]. The α form is the primary form of polypropylene obtained under normal processing conditions [2–6]; however, the β-crystal is perhaps the most interesting crystalline phase for certain applications because of its hardness and impact resistance [2–6, 8–15]. Therefore, different nucleating agents have been used to promote this type of crystal in iPP composites. In terms of nucleating agents, there are substances that contain aromatic rings, rare earth metals (referred to as WBG), and salts from dicarboxylic acids, such as calcium salts from pimelic and suberic acids [16–18]; several studies have investigated the influence of polar and non-polar parts of the nucleating agent on the formation of the β-crystal [8]. Particularly, calcium salts from pimelic and suberic acids have demonstrated an extremely high

✉ A. Almendarez-Camarillo
armando@iqcelaya.itc.mx

[1] Departamento de Ingeniería Química, Instituto Tecnológico de Celaya, Av. Tecnológico y Antonio García Cubas s/n., 38010 Celaya, Guanajuato, Mexico

[2] División de Ciencias Naturales y Exactas, Campus Guanajuato Departamento de Química, Universidad de Guanajuato, 36050 Guanajuato, Guanajuato, Mexico

[3] Departamento de Materiales Avanzados, Centro de Investigación en Química Aplicada, Blvd. Enrique Reyna Hermosillo 140, 25294 Saltillo, Coahuila, Mexico

[4] Instituto de Física, Universidad Autónoma de San Luis Potosí (IF-UASLP), Alvaro Obregón 64, 78000 San Luis Potosí, SLP, Mexico

efficiency to promote β-crystals without secondary effects [17]. Li et al. [9] studied polypropylene composites with pimelic acid (PA) and their salts to promote β-crystals. These authors reported that the salts from PA were able to induce approximately 90 % of the β growth and it also was demonstrated that the raw PA is considered an ineffective β-agent. These results agree with those obtained by Dou et al. [19], where the effect of pimelic acid and its salts, which include sodium, magnesium, zinc, calcium, barium, and aluminum, on β growth in the iPP matrix was studied. These authors found that PA and magnesium pimelate were weak β nucleators. Different substrates have been explored as supports for depositing calcium pimelate, e.g., carbonates [3, 11, 20], silicates [5, 21], zeolites [4], oxides [3], metallic salts [8, 9, 14, 22, 23], clays [24], and carbon nanotubes [6], which are responsible for more than 90 % of the β-crystals.

β nucleating agents continue as the main route to obtain β-phase in isotactic polypropylene. Several authors have studied different kinds of nucleating agents, such as multiwalled carbon nanotubes modified with calcium pimelate supported on nano $CaCO_3$ [25], monoglycerolates [26], and potassium salts [27]. In these works all of them exhibit interesting properties related to the β-phase present in the composites studied.

Although, titanium dioxide (TiO_2) has been widely used in the plastics industry (e.g., it represents >90 % of inorganic pigments and over 65 % of all colorants used in the industry) [28], the ability of this metal oxide to act as a support of β-nucleators of iPP, such as PA, has not been greatly studied and is not well understood. There are only few reports in the literature regarding this topic [3, 29]. The first study demonstrated the formation of metal pimelates due to a chemical reaction between PA and other metal oxides, except for TiO_2, based on their Infrared (IR) results. Additionally, differential scanning calorimetry (DSC) and thermogravimetric analysis (TGA) thermograms were agreed with this observation because the curves showed no differences in their melting and thermal transitions temperatures, which demonstrate that there was no chemical attachment. Additionally, the authors observed a small β diffraction peak that indicated low percentages of the β-crystal in this composite [3].

Another study made by Ahmad Zohrevand et al. [29] showed the presence of the β-structure crystals (about 60 % of β crystals with 1 % w/w of TiO_2 particles) by using TiO_2 particles which reduced the elastic modulus and yield strength of the nanocomposites. Micromechanical analysis showed an enhanced interaction between organic and inorganic phases of the compatibilized nanocomposites with anhydride-modified polypropylene.

Therefore, in this work, we propose an effective route to synthesize PA/TiO_2 nanoparticles with a high capacity to nucleate β-crystals in iPP nanocomposites. The covalent functionalization of TiO_2 was confirmed by IR spectroscopy, transmission electron microscopy (TEM), and TGA. The DSC and wide-angle X-ray diffraction (WAXD) results showed the ability of the TiO_2–PA nanofiller to ensure high β-crystal nucleation of the iPP matrix.

Materials and methods

Materials

Isotactic polypropylene (MFI = 35 g/10 min at 230 °C and 2.16 kg, ASTM D 1238) and pimelic acid (98 % purity, MW = 167 g/mol) were supplied by Sigma Aldrich. Calcium hydroxide (MW = 74.9 g/mol, 96 % purity) was supplied by Merck. Acetic acid (99 % purity, J. T.Baker), titanium *n*-butoxide (Ti(OCH4H9-*n*)$_4$) (97 % purity, Aldrich), ethanol (99 % purity, Jalmek), and sulfuric acid (97 % purity, CTR) were also used.

Synthesis of TiO_2 particles and their characterization

The TiO_2 particles were prepared according to a previous report [30]: under magnetic stirring, 20 ml of acetic acid was added drop wise to a flask containing 10 ml of titanium *n*-butoxide Ti(OC_4H_9-*n*)$_4$ diluted in 30 ml of ethanol, which was followed by the addition of 1 ml of sulfuric acid (H_2SO_4). Then, the obtained clear liquid was sonicated at 40 °C for 1 h and 60 °C for 3 h and formed a milk-like sol, which was further transferred into a 100-ml stainless steel autoclave with a Teflon inner liner and maintained at 100 °C for 13 h. The precipitates were separated from the mother liquor by centrifugation, washed thoroughly with deionized water and ethanol several times, and then dried at 100 °C in air for 12 h. Finally, the obtained powders were further calcined at 800 °C for 2 h.

The morphology and size of the TiO_2 nanoparticles were obtained using a JEOL JEM 1230 TEM microscope operated at 100 kV. The anatase form of the TiO2 nanoparticles was characterized using a Thermo Scientific DXR Raman microscope (780 nm).

Functionalization of TiO_2 nanoparticles with pimelic acid

250 mg of the previously synthesized TiO_2 nanoparticles, 100 mg of pimelic acid, and 70 mg of calcium hydroxide were mixed and sonicated for 15 min to homogenize the mixture. This mixture was subsequently pressed into an aluminum mold, sealed, heated, and held at 120 °C for 30 min. The mixture was immediately cooled in a nitrogen atmosphere until room temperature. The resulting product

was washed with 50 ml of acetone and filtered three times to remove the unbounded pimelic acid. The modified TiO_2 nanoparticles are referred to as TiO_2–PA.

Infrared spectrometry of functionalized TiO_2

IR spectra of the support (TiO_2), nucleating agent (pimelic acid), and the TiO_2–PA were obtained by Fourier transform infrared spectroscopy with an attenuated total reflection detector (FTIR-ATR Perkin, model Spectrum 100) to demonstrate the successful chemical reaction between the pimelic acid and the TiO_2 nanoparticles. The spectra were analyzed between wavenumbers of 4000 and 800 cm^{-1} with 80 scans per spectra for all samples.

Thermogravimetric analysis

The thermal stability for all samples (TiO_2, PA and TiO_2–PA) was analyzed with a TGA (TA Instruments model Q500) from 25 to 600 °C with a temperature ramp of 10 °C/min under nitrogen atmosphere. For each measurement, a sample of approximately 2 mg was placed in platinum crucibles.

Preparation of iPP/TiO_2–PA nanocomposites by melt extrusion and isothermal crystallization

iPP/TiO_2–PA and iPP/TiO_2 nanocomposites with 0.1 wt% were prepared in a co-rotating twin-screw extruder at 230 °C and 100 rpm. Conversely, the nanocomposites were isothermally crystallized in a scanning differential calorimeter (DSC, TA Instruments model Q2000) using the following temperature program: (a) the samples were heated at 10 °C/min until 200 °C, (b) held for 10 min at this temperature to erase the thermal and mechanical history, (c) then immediately cooled to 130 °C, and (d) held for 30 min at 130 °C.

WAXD measurements of the iPP, iPP/TiO_2, and iPP/TiO_2–PA nanocomposites after isothermal crystallization

The WAXD measurement for the isothermally crystallized nanocomposites was performed with an X-ray diffractometer Panalytical, X'Pert PRO model. The analysis range was between 4° and 30° using a scan rate of 4°/min. The relative amount of promoted β-crystal was determined according to standard procedures described in literature using the Turner–Teller formula [15]

$$K_\beta = \frac{H_\beta}{H_{\alpha 1} + H_{\alpha 2} + H_{\alpha 3} + H_\beta},$$

where K_β is the relative proportion of the β crystal in the sample and $H_{\alpha 1}$, $H_{\alpha 2}$, and $H_{\alpha 3}$ are the intensities of the α-diffraction peaks corresponding to angles $2\theta = 14.2°$, 17.0°, and 18.8°, respectively, and H_β is the intensity of the β-diffraction peak at $2\theta = 16.2°$.

Composites surface characterization

Topographic and phase images were obtained by atomic force microscopy (AFM) (Dimension Edge Scanning Probe Microscope, Bruker) in tapping mode using an antimony (*n*)-doped Si tip (RTESP, Bruker), whose nominal frequency and spring constant ranged between 324 and 377 kHz and 20–80 N/m, respectively. Image analysis was performed using the software Nanoscope Analysis V1.4. In the same way, a scanning electron microscope (JEOL, model JSM-820) was used in order to obtain micrographs of the composites surface to identify the position of filler particles.

Dynamical-mechanical analysis of iPP samples and its composites

The visco-elastic properties were measured using a dynamic mechanical analyzer (DMA-8000 Perkin-Elmer) in tension mode with a displacement amplitude of 0.1 mm in constant strain mode. The specimens used were rectangular sheets that were 7-mm wide, 0.5-mm thick, and 22-mm long in all cases. The temperature dependence of the storage modulus and tan δ (phase angle δ is the difference between the dynamic tension and dynamic deformation of a visco-elastic material subjected to a sinusoidal oscillation and allows for the observation of transitions, such as T_g, in which the value of tan δ against the temperature is 0, i.e., where one can observe a maximum on the graph) was measured at 10 Hz across a temperature range of −20 to 50 °C at a heating rate of 2 °C/min. The purpose of this analysis was to obtain information regarding the influence of the β-crystal content on the mechanical properties of the iPP composites. Three samples were analyzed (neat iPP, iPP/TiO_2, and iPP/TiO_2–PA).

Results and discussion

Synthesized TiO_2 particles characterization

From the TEM, we observed that the size of the particles was 266 ± 56 nm with a pseudo-spherical morphology, as shown in Fig. 1a. However, the results obtained from the Raman characterization showed that the TiO_2 obtained from the synthesis was the anatase phase, which exhibited characteristic Raman shifts at 145, 396, 515, and 636 cm^{-1}; this result is in agreement with literature [30]. The spectra are presented in Fig. 1b (inset).

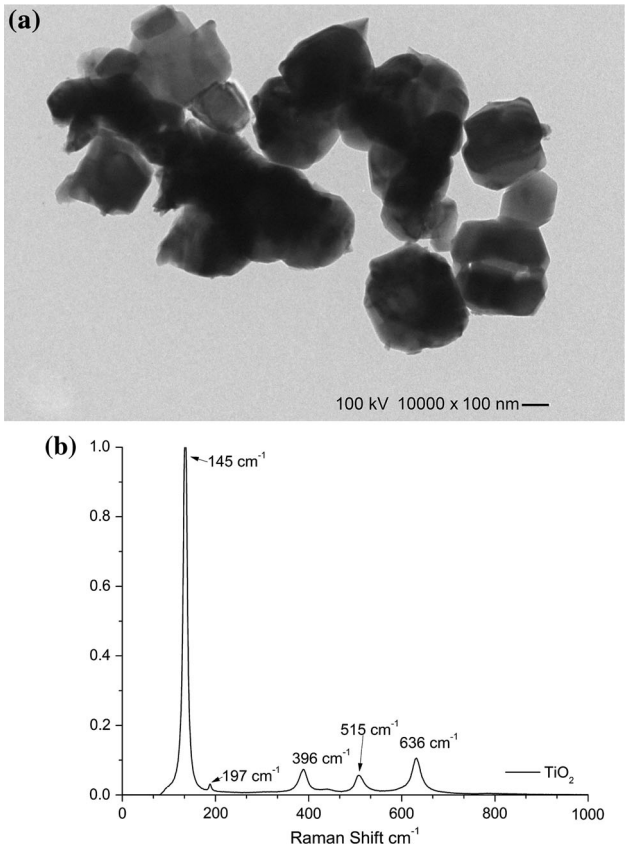

Fig. 1 TEM micrograph (**a**) and Raman spectra (**b**) from synthesized TiO_2 particles

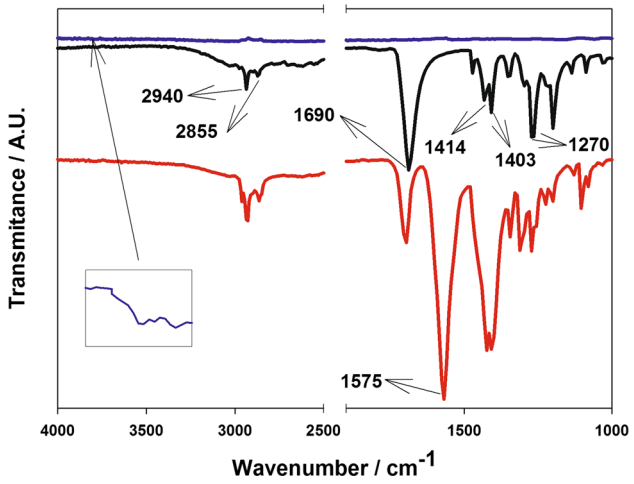

Fig. 2 IR spectra for the materials used in this study. IR spectra of the TiO_2 nanoparticles after their synthesis (*blue line*), IR spectra of the raw pimelic acid (*black line*), and IR spectra of the TiO_2–PA nanoparticles (*red line*) (Color figure online)

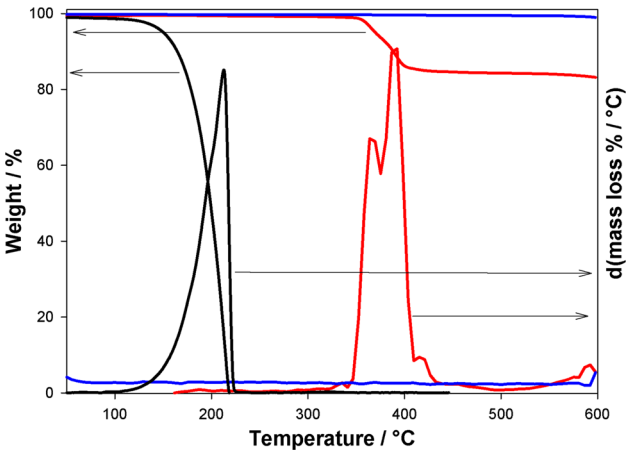

Fig. 3 TGA response during heating for all samples. *Blue line* corresponds to the TiO_2 nanoparticles, the *black line* shows the thermal decomposition and weight loss of the raw PA, and the *red line* represents the TiO_2–PA (Color figure online)

Evidence of pimelic acid attached to the TiO_2 surface (infrared measurements and thermogravimetric analysis)

Figure 2 shows the IR spectra for the TiO_2 nanoparticles, pimelic acid (PA), and TiO_2–PA (blue line, black line, and red line, respectively). A zoomed image of the IR region of 3700 and 3600 cm^{-1} shows typical IR bands for TiO_2 [31]. However, the IR spectra of the raw pimelic acid contain bands at 2940 and 2855 cm^{-1} that are related to $-CH_2$ stretching (υ_{C-H}); the band at 1690 cm^{-1} can be attributed to the carbonyl group stretching ($\upsilon_{C=O}$), and vibrations at 1414 and 1270 cm^{-1} are attributed to C–O–H in-plane bending (δ_{C-O-H}) and stretching vibrations (υ_{C-O}), respectively. After the chemical functionalization process, the peak at 1403 cm^{-1} continues to appear in the FTIR spectra, and a new band at 1575 cm^{-1} emerged; according to the literature, this observation can be attributed to asymmetric (v_{asym}) and symmetric (v_{sym}) stretching vibrations of the carboxylate group (COO^-), respectively. Other reports indicate that this band at 1575 cm^{-1} indicates a bond between pimelic acid molecules and metal ions [24, 32]. The last observation and the fact that the IR spectrum of the TiO_2–PA does not show any changes after being washed with acetone indicate that PA molecules were successfully attached to the TiO_2 surface [8, 33, 34].

Successful chemical bonding between PA molecules and inorganic support surfaces thermally stabilizes molecules, which has been observed when PA molecules have been bound to clays, carbon nanotubes, and even other metal oxides [2, 3, 6, 35]. Figure 3 shows the TGA thermograms for each sample. The TiO_2 nanoparticles exhibit a high thermal stability without changes until 600 °C (see blue line), which agrees with that in literature [3]. In contrast, the PA thermogram has an important transition between 110 and 225 °C with a maximum peak at 212 °C

(see black line). This transition can be attributed to the phase change of this organic molecule [2, 3]. Finally, the thermal degradation of the TiO_2–PA sample occurs in two steps with maximum at 365 and 390 °C; in this step, the evaporation of organic substances occurs as cyclohexanone is produced by the decomposition of bounded PA. These transitions are typically attributed to the evaporation of organic substances produced by the decomposition of pimelic acid [2, 5, 35]. An interesting observation is that the thermal stability of pimelic acid occurred at a greater temperature (at 180 °C in comparison with that of raw pimelic acid molecules). This is likely because the pimelic acid molecules were chemically attached to the support (TiO_2 nanoparticles) [2, 3, 5, 36]. The percentage of supported PA on the TiO_2 surface according to this analysis was approximately 15 % by weight.

Evidence of β-crystals in the iPP nanocomposite by DSC and WAXD

Figure 4a, b shows the DSC thermograms and WAXD patterns of the isothermally crystallized composites, respectively. As iPP melts (Fig. 4a, blue line), a unique thermal transition was observed in the region between 156 and 168 °C with a maximum peak at 164 °C. This transition is attributed to the melting of the α phase [3, 9]; however, the thermograms of the iPP nanocomposites (Fig. 4a, red line and black line) show a bimodal behavior with a new peak at 152 °C, which is normally attributed to the melting of the β crystal [14, 37, 38]. Additionally, this peak increased for the iPP nanocomposites when the TiO_2 nanoparticles were functionalized with PA. This behavior has been observed when PA has been attached to other supports, such as carbon nanotubes, nanoclay, nanocarbonates, etc. [1, 5, 36]. However, there have been no reports on using TiO_2 to support PA molecules that contained an endotherm of the β-crystal during the melting of iPP composites [3]. In the same way, Fig. 4b shows an increase of the characteristic diffraction peak at $2\theta = 16.2$ β(300) that is attributed to the β-crystal for the iPP/TiO_2–PA nanocomposite [39]. The K_β value obtained in the present report was approximately 85 %, which is in contrast to the 0.9 % reported in literature [3]; this result indicates the high β-nucleating ability of the TiO_2/PA support that was synthesized to promote the nucleation of the β-crystal phase. The K_β values of the nucleated samples are provided in Table 1. In this table, we provide the total crystallinity value for the samples; here it can be observed that there are no significant changes between the samples studied. This could be attributed to the low amount of filler particles used in this work.

Surface morphology of iPP and its composites by atomic force microscopy (AFM) and scanning electron microscope (SEM)

Atomic force microscopy (AFM) was performed to quantify the roughness of the materials and topography using intermittent contact with the surface of the composites. Figure 5 shows the surface of the sample that contains as a filler, the modified particles with pimelic acid (iPP/TiO_2–PA), which exhibit a homogeneous topography compared with that of the iPP/TiO_2 composite. Furthermore, an analysis by the computer software was used to estimate the roughness values of the samples, which are shown in Table 2. In this table, it can be observed that the neat iPP had the lowest roughness compared with the nanocomposites, which is because only iPP chains are present in the bulk and those have a highly elastic behavior [40]. However, for the composites containing non-functional titanium dioxide (iPP/TiO_2), the incompatibility of TiO_2 particles with the iPP matrix becomes evident from the

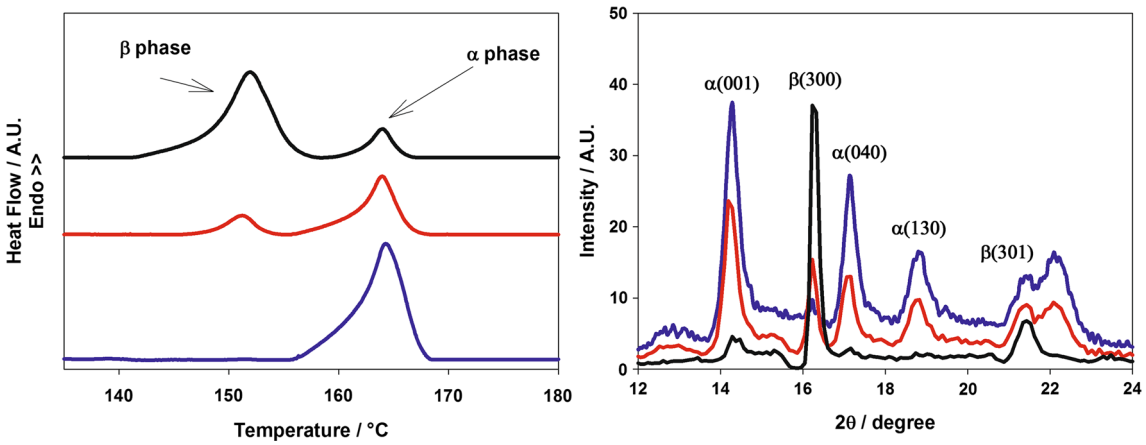

Fig. 4 *Left side* shows the DSC thermograms for all samples **a** raw iPP, **b** iPP/TiO_2, and **c** iPP/TiO_2–PA nanocomposite. *Right side* shows their WAXD patterns: raw iPP (*blue line*), iPP/TiO_2 (*red line*), and iPP/TiO_2–PA (*black line*) nanocomposite (Color figure online)

Table 1 Total crystallinity of studied samples and amount of β-crystal quantified by DSC and WAXD for iPP and the nanocomposites at 0.1 % w/w of iPP/TiO_2 and iPP/TiO_2–PA

Sample	Amount of filler (w/w %)	Total crystallinity (%)	β crystal (%) by DSC	β crystal (%) by WAXD
iPP	0	49.3	0.7	5.2
iPP/TiO_2	0.1	54.2	21.7	25
iPP/TiO_2–PA	0.1	53.2	85.7	85.3

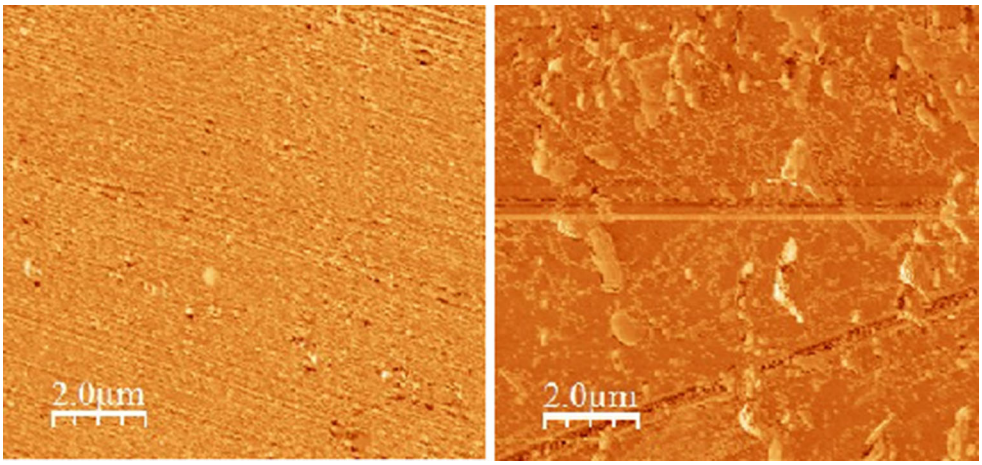

Fig. 5 AFM topography image for iPP composites: iPP/TiO_2–PA (*left*) and iPP/TiO_2 (*right*)

Table 2 Surface roughness of all studied samples from AFM measurements

	iPP	iPP/TiO_2–PA	iPP/TiO_2
R_q (root mean squared)	2.64	5.56	6.82
R_a (arithmetic average)	1.73	4.26	5.14

topographical image; the protruding reliefs are attributed to oxide particles that migrate to the material surface by exclusion when the iPP matrix crystallized [40, 41]. In contrast with these observations, the iPP/TiO_2–PA sample had a homogeneous surface that indicates a favorable dispersion that could prevent cluster formation at the surface level and a better integration into the polymer matrix. In this case, the PA molecules that chemically link to the TiO_2 particles act as nuclei centers and improve the integration of particles inside the polymer matrix. These observations are concomitant with the SEM images in Fig. 6a, where iPP/TiO_2 composite shows excluded particles on their surface (in red circles), while the iPP/TiO_2–PA composites show an homogeneous surface without cluster formation evidence (See blue circle in Fig. 6b).

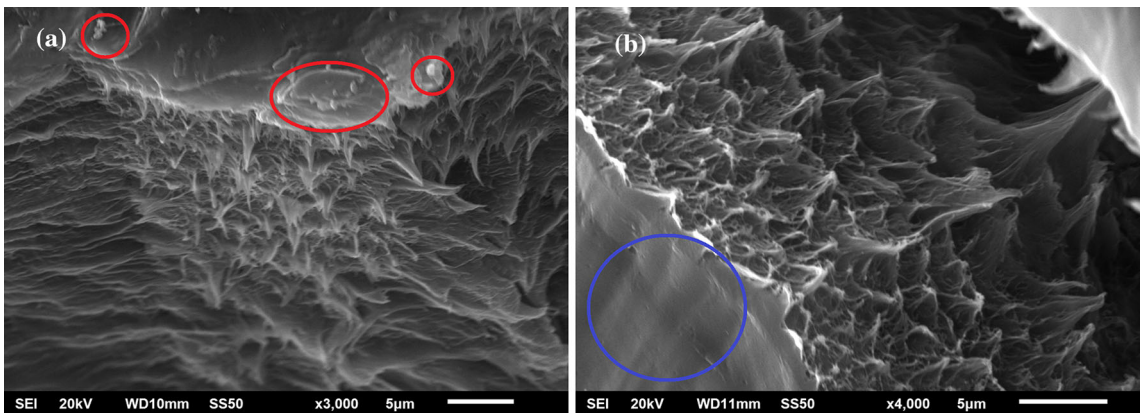

Fig. 6 SEM micrographs of iPP/TiO_2 (**a**) and iPP/TiO_2–PA (**b**) composites. In *red circles* are shown the agglomeration of TiO_2 particles on iPP/TiO_2 composite surface and in *blue circle* the homogenous surface of iPP/TiO_2–PA composite (Color figure online)

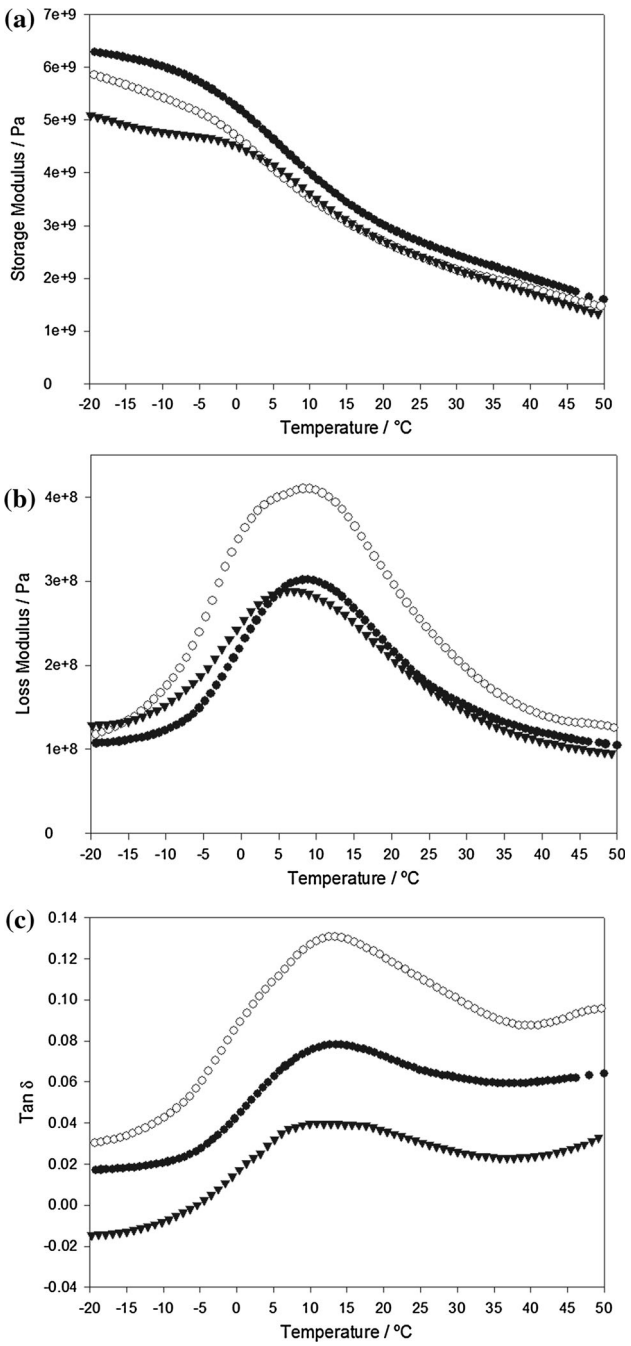

Fig. 7 Storage modulus response (**a**), loss modulus response (**b**), and loss factor behavior (tan δ) in the DMA analysis for neat iPP (*black triangles*) and composites iPP/TiO_2 (*black circles*) and iPP/TiO_2–PA (*white circles*)

Effect of β-crystals on the visco-elastic properties of iPP and its nanocomposites

A DMA study was performed to measure the dynamic response of the samples under stretching at a constant periodic rate. The visco-elastic behavior of polymer nanocomposites, particularly the glass transition state, is a key factor in understanding the relation between the structural properties of the materials and their processing properties.

Figure 7a shows the storage modulus behavior with temperature (−20 to 50 °C) for the three samples studied. This figure shows that the storage modulus increased by the addition of both types of nanoparticles (TiO_2 and TiO_2–PA) into the iPP matrix, even at low percentages (<0.1 % w/w). The increase in the storage modulus is related to the mechanical reinforcement provided by the modified and unmodified titanium dioxide particles on the iPP matrix [35, 42, 43].

Several differences were observed in the storage modulus behavior for both iPP/TiO_2 and iPP/TiO_2–PA composites with the temperature scan, even when both contained the same percentage of TiO_2. This change in storage modulus at the beginning of the experiment could be attributed to two phenomenal combination: (1) the slight increment of total crystallinity in iPP/TiO2 composite, because the composite stiff is related to the amount of crystals in semicrystalline polymers and (2) the different nucleation crystal behaviors of the iPP of each type of nanocomposite because α-crystals have a higher rigidity compared with that of the β-crystals. Therefore, the iPP/TiO_2 sample exhibits a greater storage modulus compared with that of its counterpart that is rich in β according to previous DSC and WAXD results (iPP/TiO_2–PA) [35, 44, 45].

Additionally, when the temperature increased, the material exhibits less elastic behavior and begins to be dominated by viscous behavior; this change was reflected by a decrease in the storage modulus as the temperature increased for all samples.

Likewise, the study on the loss modulus of these materials provides information regarding the amount of energy dissipated by the samples as internal friction or molecular movements and this can be used as a measure of the behavior of the viscous component of the material, which is attributed to the unrecoverable oscillatory energy that is dissipated per cycle [42, 46, 47]. From Fig. 7b, an increase in the value of the loss modulus can be observed when the β lamellae is promoted and the nucleating TiO_2–PA particles are coupled and homogeneously dispersed in the polymer matrix, which helps it to dissipate the energy around itself and is similar to the inside of the plastic matrix during visco-elastic deformation [46, 47]. These observations agree with the AFM results, where the iPP/TiO_2–PA sample exhibited a homogeneous surface. The loss modulus reached a peak when it was close to the glass transition temperature and suddenly decreased, which indicates that the flow movement of the chains increased above the transition temperature (see Fig. 7b).

The storage modulus and loss modulus are greater for the reinforced samples compared with those of the unfilled iPP; this behavior has been observed previously in other systems where the polymer matrix contains reinforcing

Table 3 Glass transition temperatures (T_g) obtained by DMA measurements of unfilled iPP and nanocomposites at 0.1 % w/w of iPP/TiO_2 and iPP/TiO_2–PA

Sample	T_g (°C)
iPP	10.9 ± 0.2
iPP/TiO_2	13.4 ± 0.1
iPP/TiO_2–PA	13.8 ± 0.1

materials. In these studies, the primary concern was the influence of the filler on the molecular motion of the crystalline region [35, 42, 43]. Because the β-phase relation with the improvement of the impact strength in polypropylene systems is clear in Fig. 7a, the iPP/TiO2–PA composite (with a high content of this crystalline form) must display an increase in the dissipation of energy, which the DMA measurements indicated [35].

Lastly, Fig. 7c shows the behavior of the tan δ as a function of temperature for all samples. The peak value for the function of tan δ obtained by the DMA software (Perkin-Elmer) is attributed to the glass transition temperature (T_g) of the material. A T_g of 10.9 °C was obtained for the neat iPP and for the iPP/TiO_2 and iPP/TiO_2–PA composites, it was 13 and 13.5 °C, respectively (see Table 3).

The value of T_g tended to shift to the right by the effect of the particles in the plastic matrix because the mobility between adjacent chains is affected by the presence of the fillers [35, 42, 43, 46, 47]. Still, there is a difference between the iPP/TiO_2–PA composite and iPP/TiO_2 despite both containing the same percentage of loading filler (0.1 % w/w). An increase in the glass transition temperature for the iPP/PA–TiO_2 composite can be attributed to the increased fraction of tie points through the amorphous layers located between the β lamella; this phenomenon immobilizes the chains in the amorphous phase within the β lamellae crystals. Furthermore, the interaction of the non-polar part of the PA molecules with the iPP chains organized in β form could decrease the chain mobility at the interface of the modified particles.

Conclusions

In this work, we modified a common filler of iPP, i.e., titanium oxide, by chemical functionalization with a very selective β-nucleating agent (pimelic acid) through an effective synthesis route resulting in a highly thermally stable filler that is able to promote the important crystalline phase of iPP (β-crystal) at low percentages of functionalized nanoparticles (0.1 % w/w). It was found that about 85 % of β-crystal content was promoted with the TiO_2–PA particles. From the loss modulus behavior, it is evident that a higher β-crystal induction in the iPP/TiO_2–PA composites helps to dissipate energy during oscillation deformation. The improvement in the ability to dissipate energy of the β-crystal could be then related to the improved impact strength of the iPP matrix. It was concluded that our chemical functionalization route of TiO_2 particles with PA molecules promotes the dispersion of particles into the composites, which enhances the visco-elastic properties of polypropylene. In the industry, this chemical modification could enhance the integration of titanium dioxide particles with the plastic matrix and in the same way improve its properties to dissipate energy in the composite.

Acknowledgements This work was partially supported by Conacyt and DGEST through grants 78904 and 5207.14- P, respectively. J.A.G-C thanks Conacyt for Ph.D. scholarship 237999.

References

1. Varga J, Mudra I, Ehrenstein GW (1999) Crystallization and melting of β-nucleated isotactic polypropylene. J Therm Anal Calorim 56:1047–1057. doi:10.1023/A:1010132306934
2. Dai X, Zhang Z, Wang C, Ding Q, Jiang J, Mai K (2013) A novel montmorillonite with β-nucleating surface for enhancing β-crystallization of isotactic polypropylene. Composites Part A 49:1–8. doi:10.1016/j.compositesa.2013.01.016
3. Zhang Z, Wang C, Junping Z, Mai K (2012) β-Nucleation of pimelic acid supported on metal oxides in isotactic polypropylene. Polym Int 61:818–824. doi:10.1002/pi.4148
4. Jiang J, Li G, Tan N, Ding Q, Mai K (2012) Crystallization and melting behavior of isotactic polypropylene composites filled by zeolite supported β-nucleator. Thermochim Acta 546:127–133. doi:10.1016/j.tca.2012.07.032
5. Ding Q, Zhang Z, Wang C, Jiang J, Li G, Mai K (2012) Crystallization behavior and melting characteristics of wollastonite filled β -isotactic polypropylene composites. Thermochim Acta 536:47–54. doi:10.1016/j.tca.2012.02.023
6. Wang S-W, Yang W, Bao R-Y, Wang B, Xie B-H, Yang M-B (2010) The enhanced nucleating ability of carbon nanotube-supported β -nucleating agent in isotactic polypropylene. Colloid Polym Sci 288:681–688. doi:10.1007/s00396-010-2194-x
7. Bikiaris D, Vassiliou A, Chrissafis K, Paraskevopoulos KM, Jannakoudakis A, Docoslis A (2008) Effect of acid treated multiwalled carbon nanotubes on the mechanical, permeability, thermal properties and thermo-oxidative stability of isotactic polypropylene. Polym Degrad Stab 93:952–967. doi:10.1016/j.polymdegradstab.2008.01.033
8. Li X, Hu K, Ji M, Huang Y, Zhou G (2002) Calcium dicarboxylates nucleation of β-polypropylene. J Appl Polym Sci 86:633–638. doi:10.1002/app.10913
9. Li JX, Cheung WL (1997) Pimelic acid-based nucleating agents for hexagonal crystalline polypropylene. J Vinyl Addit Technol 3:151–156. doi:10.1002/vnl.10182
10. Li JX, Cheung WL (1999) Conversion of growth and recrystallisation of β-phase in doped iPP. Polymer 40:2085–2088. doi:10.1016/S0032-3861(98)00425-X
11. Zhang Z, Wang C, Meng Y, Mai K (2012) Synergistic effects of toughening of nano-$CaCO_3$ and toughness of β-polypropylene. Composites Part A 43:189–197. doi:10.1016/j.compositesa.2011.10.008
12. Duan J, Dou Q (2012) Investigation on β-polypropylene/PP- g -MAH/surface-treated calcium carbonate composites. Polym Compos 33:2245–2261. doi:10.1002/pc.22370
13. Dou Q, Meng MR, Li L (2010) Effect of pimelic acid treatment on the crystallization, morphology, and mechanical properties of

isotactic polypropylene/mica composites. Polym Compos 31:1572–1584. doi:10.1002/pc.20945
14. Li J, Cheung W, Jia D (1999) A study on the heat of fusion of β-polypropylene. Polymer (Guildf) 40:1219–1222. doi:10.1016/S0032-3861(98)00345-0
15. Somphon W, Haller KJ (2013) Crystal growth and physical characterization of picolinic acid cocrystallized with dicarboxylic acids. J Cryst Growth 362:252–258
16. Ivanov E, Valiev KA (2007) The problem of nucleation of polypropylene (Review). Plast Massy 11–15. http://search.proquest.com/openview/47641416b41d5dbd5c810aa09d52183a/1?pq-origsite=gscholar
17. Xiao W, Wu P, Feng J (2008) Effect of β-nucleating agents on crystallization and melting behavior of isotactic polypropylene. J Appl Polym Sci 108:3370–3379. doi:10.1002/app.27997
18. Varga J (2002) β-modification of isotactic polypropylene: preparation, structure, processing, properties, and application. J Macromol Sci Part B 41:1121–1171. doi:10.1081/MB-120013089
19. Dou Q (2007) Effect of metallic salts of pimelic acid and crystallization temperatures on the formation of β crystalline form in isotactic polypropylene. J Macromol Sci Phys 46:1063–1080. doi:10.1080/00222340701581334
20. Gahleitner M, Grein C, Bernreitner K (2012) Synergistic mechanical effects of calcite micro- and nanoparticles and β-nucleation in polypropylene copolymers. Eur Polym J 48:49–59. doi:10.1016/j.eurpolymj.2011.10.013
21. Meng MR, Dou Q (2008) Effect of pimelic acid on the crystallization, morphology and mechanical properties of polypropylene/wollastonite composites. Mater Sci Eng A 492:177–184. doi:10.1016/j.msea.2008.03.048
22. Li JX, Cheung WL (1999) Conversion of growth and recrystallisation of β-phase in doped iPP. Polymer (Guildf) 40:2085–2088. doi:10.1016/S0032-3861(98)00425-X
23. Lee CYC, Hines AL (1987) Adsorption of glutaric, adipic, and pimelic acids on activated carbon. J Chem Eng Data 32:395–397. doi:10.1021/je00050a001
24. Dai X, Zhang Z, Wang C, Ding Q, Jiang J, Mai K (2013) A novel montmorillonite with β-nucleating surface for enhancing β-crystallization of isotactic polypropylene. Composites Part A 49:1–8. doi:10.1016/j.compositesa.2013.01.016
25. Chen C, Z Zhang, Ding Q, Wang C, Mai K (2014) Influence of different β-nucleating agent on crystallization behavior, morphology, and melting characteristic of multiwalled carbon nanotube-filled isotactic polypropylene nanocomposites. Polym Compos 36(4):635–643. doi:10.1002/pc.22981
26. Bhatia A, Jayaratne VN, Simon GP, Edward GH, Turney TW (2015) Nucleation of isotactic polypropylene with metal monoglycerolates. Polymer 59:110–116. doi:10.1016/j.polymer.2014.12.038
27. Jiang C, Zhao S, Xin Z (2015) Influence of a novel β-nucleating agent on the structure, mechanical properties, and crystallization behavior of isotactic polypropylene. J Thermoplast Compos Mater 28(5):610–619. doi:10.1177/0892705713486139
28. Maier C, Calafut T (1998) Polypropylene: the definitive users guide and handbook. Plastic Design Library, William Andrew Inc., New York
29. Zohrevand A, Ajji A, Mighri F (2014) Morphology and properties of highly filled iPP/TiO_2 nanocomposites. Polym Eng Sci 54(4):874–886. doi:10.1002/pen.23625
30. Tong T, Zhang J, Tian B, Chen F, He D (2008) Preparation and characterization of anatase TiO_2 microspheres with porous frameworks via controlled hydrolysis of titanium alkoxide followed by hydrothermal treatment. Mater Lett 62:2970–2972. doi:10.1016/j.matlet.2008.01.085
31. Primet M, Pichat P, Mathieu MV (1971) Infrared study of the surface of titanium dioxides. I. Hydroxyl groups. J Phys Chem 75:1216–1220. doi:10.1021/j100679a007
32. Mitra T, Sailakshmi G, Gnanamani A, Mandal AB (2013) The effect of pimelic acid interaction on the mechanical and thermal properties of chitosan and collagen. Int J Polym Mater 62:572–582. doi:10.1080/00914037.2013.769161
33. Taguchi M, Takami S, Naka T, Adschiri T (2009) Growth mechanism and surface chemical characteristics of dicarboxylic acid-modified CeO_2 nanocrystals produced in supercritical water: tailor-made water-soluble CeO_2 nanocrystals. Cryst Growth Des 9:5297–5303. doi:10.1021/cg900809b
34. Kazuo N (2006) Infrared and Raman spectra of inorganic and coordination compounds. Handb. Vib. Spectrosc. Wiley, Chichester
35. Gonzalez-Calderon JA, Castrejon-Gonzalez EO, Medellin-Rodriguez FJ, Stribeck N, Almendarez-Camarillo A (2014) Functionalization of multi-walled carbon nanotubes (MWCNTs) with pimelic acid molecules: effect of linkage on β-crystal formation in an isotactic polypropylene (iPP) matrix. J Mater Sci 50:1457–1468. doi:10.1007/s10853-014-8706-1
36. Zhang Z, Tao Y, Yang Z, Mai K (2008) Preparation and characteristics of nano-$CaCO_3$ supported β-nucleating agent of polypropylene. Eur Polym J 44:1955–1961. doi:10.1016/j.eurpolymj.2008.04.022
37. Li JX, Cheung WL, Chan CM (1999) On deformation mechanisms of β-polypropylene 2. Changes of lamellar structure caused by tensile load. Polymer (Guildf) 40:2089–2102. doi:10.1016/S0032-3861(98)00412-1
38. Lotz B (1998) α and β phases of isotactic polypropylene: a case of growth kinetics 'phase reentrency' in polymer crystallization. Polymer (Guildf) 39:4561–4567. doi:10.1016/S0032-3861(97)10147-1
39. Huo H, Jiang S, An L, Feng J (2004) Influence of shear on crystallization behavior of the β phase in isotactic polypropylene with β-nucleating agent. Macromolecules 37:2478–2483. doi:10.1021/ma0358531
40. Lin Q-B, Li H, Zhong H-N, Zhao Q, Xiao D-H, Wang Z-W (2014) Migration of Ti from nano-TiO_2-polyethylene composite packaging into food simulants. Food Addit Contam Part A. doi:10.1080/19440049.2014.907505
41. Thomas SP, Thomas S, Bandyopadhyay S (2009) Mechanical, atomic force microscopy and focussed ion beam studies of isotactic polystyrene/titanium dioxide composites. Composites Part A 40:36–44. doi:10.1016/j.compositesa.2008.10.005
42. Venkatesh GS, Deb A, Karmarkar A, Chauhan SS (2012) Effect of nanoclay content and compatibilizer on viscoelastic properties of montmorillonite/polypropylene nanocomposites. Mater Des 37:285–291. doi:10.1016/j.matdes.2011.12.034
43. Laoutid F, Estrada E, Michell RM, Bonnaud L, Müller AJ, Dubois Ph (2013) The influence of nanosilica on the nucleation, crystallization and tensile properties of PP-PC and PP–PA blends. Polymer (United Kingdom) 54:3982–3993. doi:10.1016/j.polymer.2013.05.031
44. Tjong SC, Shen JS, Li RKY (1996) Mechanical behavior of injection molded β-crystalline phase polypropylene. Polym Eng Sci 36:100–105. doi:10.1002/pen.10390
45. Jacoby P, Bersted BH, Kissel WJ, Smith C (1986) Studies on the β-crystalline form of isotactic polypropylene. J Polym Sci Part B 24:461–491. doi:10.1002/polb.1986.090240301
46. Rong MZ, Zhang MQ, Pan SL, Lehmann B, Friedrich K (2004) Analysis of the interfacial interactions in polypropylene/silica nanocomposites. Polym Int 53:176–183. doi:10.1002/pi.1307
47. Labour T, Vigier G, Séguéla R, Gauthier C, Orange G, Bomal Y (2002) Influence of the β-crystalline phase on the mechanical properties of unfilled and calcium carbonate-filled polypropylene: ductile cracking and impact behavior. J Polym Sci Part B 40:31–42. doi:10.1002/polb.10068